Title: Emergent constraints on the sensitivity of global land surface runoff to temperature based on CMIP6 projections

Authors: Yuanfang Chai[1], Wouter R. Berghuijs[1], Yue Yao[2], Thomas A.J. Janssen[1] and Han Dolman[1,3*]

[1] Department of Earth Sciences, Free University Amsterdam, Netherlands.

[2] State Key Laboratory of Water Resources and Hydropower Engineering Science, School of Water Resources and Hydropower Engineering, Wuhan University, Wuhan, 430072 China

[3] School of Geography, Nanjing University of Science and Technology, Nanjing, China.

Corresponding author: Han Dolman

Address: Department of Earth Sciences, Free University Amsterdam, Netherlands.

Tel: +31-20-5987358

Email: han.dolman@vu.nl

ORCIDS: http://orcid.org/0000-0003-0099-0457

1. Data

To investigate the performance of CMIP6 models and to estimate the uncertainties in $\Delta R/\Delta T$, we collected monthly temperature, precipitation and land surface runoff from the 21 CMIP6 models (https://esgf-node.llnl.gov/projects/cmip6/, Table S1) both for the historical period (1979 – 2014) and for the future (2015 – 2100) under the emission scenarios of SSP126, SSP245, SSP370 and SSP585 (O'Neill et al., 2016). We collected temperature and precipitation observations from the HadCRUT5 data set (http://www.cru.uea.ac.uk/), and observation-based Global Composite Runoff Fields and observed runoff in the 120 large rivers from the Global Runoff Data Centre (https://www.bafg.de/GRDC/EN/Home/homepage_node.html, Fekete et al., 2002). We collected monthly temperature, precipitation and land surface runoff values of 17 CMIP5 models (Table S2) for the historical period and the future period under the emission scenarios of RCP2.6, RCP4.5, RCP6.0, and RCP8.5 (https://esgf-node.llnl.gov/search/cmip5/, Taylor et al., 2012). We regridded all the CMIP5 and CMIP6 outputs to a common 0.25° × 0.25° latitude-longitude spatial resolution by using nearest neighbor interpolation method for calculating the CMIP6 multi-model mean values.

Poor simulation of other hydrological variables (precipitation, snow melt, soil water content and evaporation) can cause large uncertainties of $\Delta R/\Delta T$ in each CMIP6 models. Therefore, to identify the dominant factor causing spread in the future $\Delta R/\Delta T$ across CMIP6 models through investigating regression relationships of future $\Delta R/\Delta T$ with other hydrological variables, monthly data of precipitation from 21 CMIP6 models, snow melting runoff from 16 CMIP6 models (Table S3), soil water content from 21 CMIP6 models (Table S4) and total evaporation from 19 CMIP6 models (Table S5) under the four emission scenarios of SSP126, SSP245, SSP370 and SSP585 are collected from https://esgf-node.llnl.gov/projects/cmip6/.

To investigate the implications of the constrained $\Delta R/\Delta T$ on extreme rainfall events, the daily data of precipitation from 10 CMIP6 models (Table S6) under the four emission scenarios SSP126, SSP245, SSP370 and SSP585 is also collected from the CMIP6 database. To verify that our main findings are not dependent on a specific observational data set, we also collected the other two data sets, namely "GPCC and HadCRUT5" (https://www.cgd.ucar.edu/cas/catalog/surface/precip/gpcc.html) and the "GISS and GPCC" (https://www.esrl.noaa.gov/psd/data/gridded/data.gistemp.html), used for deriving $\Delta P/\Delta T$ from observations.

2. Methods

2.1 Emergent constraint method

Earth system models are widely used to predict future climate changes at regional to global scale, but these climate projections have large uncertainties (Knutti et al., 2013). The "emergent constraint" method has been developed to reduce such uncertainties (Hall et al., 2006). Specifically, the emergent constraint method consists of a physically-explainable empirical relationship between the inter-model spread of an historical observable variable (namely "independent variable x") and the inter-model spread of a future climate predicted variable (namely "dependent variable y") (Cox et al., 2018; Chai et al., 2021). The "independent variable x" ideally is well enough observed to provide an accurate mean state, variability or variation trend (Klein et al., 2015). By projecting the observed estimate of the "independent variable x" with its observational uncertainty (±one standard deviation) onto the y-axis through the empirical linear relationship, a more reliable and accurate "dependent variable y" with hopefully narrower uncertainties can be obtained (Brient et al., 2020). Importantly, because empirical relationships could just be fortuitous, a plausible physical mechanism is a fundamental requirement for the underlying empirical relationship (Hall et al., 2019).

2.2 Building an emergent constraint relationship

We use the least-squares linear regression method to build the emergent constraint relationships (Chai et al., 2021). The 'prediction error' of the regression is σ_y, calculated by equation (1); *y(x)* is the linear regression equation (2);

$$\sigma_{y(x)} = s\sqrt{1+\frac{1}{N}+\frac{(x-\bar{x})^2}{N\cdot\sigma_x^2}} \tag{1}$$

$$y_i = ax_i + b \tag{2}$$

where y_i (future global annual average $\Delta R/\Delta T$) is the value given by x_i (historical observed global annual average $\Delta P/\Delta T$); a and b are the slope and intercept, respectively; s is used for minimizing the least-squares error, calculated by equation (3); and N is the number of data points (number of models). σ_x is the variance of x_i, calculated by equation (4); $\bar{x}$ is the mean value;

$$s^2 = \frac{1}{N-2}\sum_{n=1}^{N}(y-y_i)^2 \tag{3}$$

$$\sigma_x = \sqrt{\sum_{n=1}^{N}(x_i-\bar{x})^2 / N} \tag{4}$$

2.3 Calculation of probability density

Based on the assumption that all model simulations are equally likely and form a Gaussian distribution (Kwiatkowski et al., 2017), we calculate the probability density function (PDF) for the original inter-model spread of the future global annual average $\Delta R/\Delta T$ (y) using equation (5).

$$PDF(y/x) = \frac{1}{\sqrt{2\pi\cdot\sigma_y^2}}\exp\left\{-\frac{(y-f(x))^2}{2\sigma_y^2}\right\} \tag{5}$$

where *PDF(y/x)* is the probability density function around the best-fit linear regression, which represents the estimated probability density of y given x.

We use the equation (6) to calculate the PDF for the constrained future global annual average $\Delta R/\Delta T$ (y). Where *PDF(F/H)* is the probability density of "future global annual average $\Delta R/\Delta T$ (y)" given "historical observable global annual average $\Delta P/\Delta T$ (x)"; *PDF(H)* is the observation-based PDF for "observed global annual average $\Delta P/\Delta T$ (x)"; Thus, after the emergent constraint, the PDF for "the constrained future global annual average $\Delta R/\Delta T$ (y)" (*PDF(F)*) is calculated by numerically integrating *PDF(F/H)* and *PDF(H)*.

$$PDF(F) = \int_{-\infty}^{+\infty} PDF(F/H) \cdot PDF(H) \cdot dH \qquad (6)$$

2.4 Definition and calculation of annual heavy and light rain days

Changes in heavy and light rainfall days can directly affect land surface runoff, leading to a tight relationship between these variables. After obtaining the constrained global annual average $\Delta R/\Delta T$, this relationship, combined with the constrained $\Delta R/\Delta T$, is used to investigate the future changes in heavy and light rainfall days, which would be an indication for future changes of global average dry and wet conditions. Extreme light and heavy rainfall days here are defined as the days with rainfall (including days without rainfall) lower than the long-term 10th percentile and the rainfall higher than long-term 90th percentile, respectively. Based on the outputs of the daily precipitation during 2015 – 2100 from 12 CMIP6 models, we estimated the annual light and heavy rainfall days in each grid. The mean value of the annual light and heavy rainfall days in all terrestrial grids is regarded as the global average number of annual drought days and heavy rainfall days.

References

Brient, F. (2020). Reducing uncertainties in climate projections with emergent constraints: Concepts, Examples and Prospects. *Advances in Atmospheric Sciences*, **37**(1), 1-15. https://doi.org/10.1007/s00376-019-9140-8

Chai, Y., Martins, G., Nobre, C., Randow, C., Chen, T., & Dolman, H. (2021). Constraining Amazonian land surface temperature sensitivity to precipitation and the probability of forest dieback. *npj Climate Atmospheric Science*, **4**, 6.

Cox, P. M., Huntingford, C., & Williamson, M. S. (2018). Emergent constraint on equilibrium climate sensitivity from global temperature variability. *Nature*, **553**(7688), 319-322. https://doi.org/10.1038/nature25450

Fekete, B. M., Vörösmarty, C. J., & Grabs, W. (2002). High-resolution fields of global runoff combining observed river discharge and simulated water balances. *Global Biogeochemical Cycles*, **16**(3), 15-1. https://doi.org/10.1029/1999GB001254

Hall, A., & Qu, X. (2006). Using the current seasonal cycle to constrain snow albedo feedback in future climate change. *Geophysical Research Letters*, **33**(3), L03502. https://doi.org/10.1029/2005GL025127

Hall, A., Cox, P., Huntingford, C., & Klein, S. (2019). Progressing emergent constraints on future climate change. *Nature Climate Change*, **9**(4), 269-278. https://doi.org/10.1038/s41558-019-0436-6

Klein, S. A., & Hall, A. (2015). Emergent constraints for cloud feedbacks. *Current Climate Change Reports*, **1**(4), 276-287. https://doi.org/10.1007/s40641-015-0027-1

Kwiatkowski, L., Bopp, L., Aumont, O., Ciais, P., Cox, P. M., Laufkötter, C., et al. (2017). Emergent constraints on projections of declining primary production in the tropical oceans. *Nature Climate Change*, **7**(5), 355-358. https://doi.org/10.1038/nclimate3265

O'Neill, B. C., Tebaldi, C., Vuuren, D. P. V., Eyring, V., Friedlingstein, P., Hurtt, G., et al. (2016). The scenario model intercomparison project (ScenarioMIP) for CMIP6. *Geoscientific Model Development*, **9**(9), 3461-3482. https://doi.org/10.5194/gmd-9-3461-2016

Taylor, K. E., Stouffer, R. J., & Meehl, G. A. (2012). An overview of CMIP5 and the experiment design. *Bulletin of the American meteorological Society*, **93**(4), 485-498. https://doi.org/10.1175/BAMS-D-11-00094.1

Knutti, R., & Sedláček, J. (2013). Robustness and uncertainties in the new CMIP5 climate model projections. *Nature Climate Change*, **3**(4), 369-373. https://doi.org/10.1038/nclimate1716

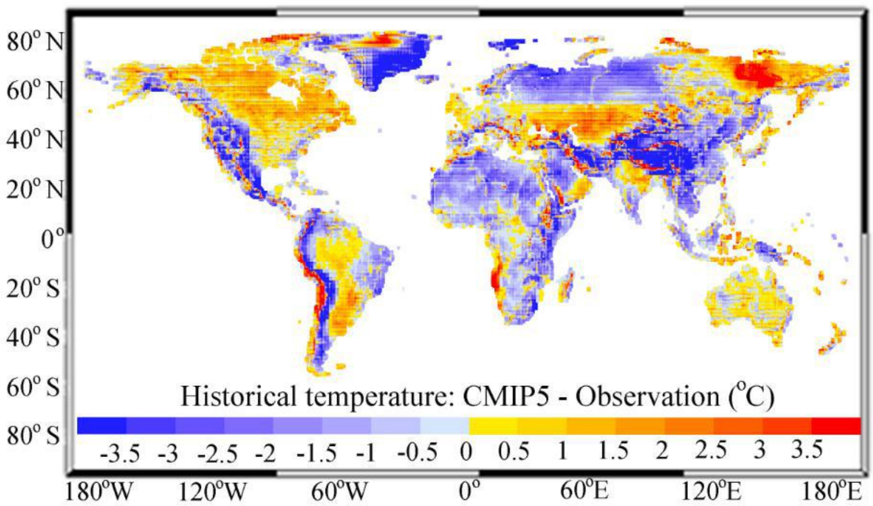

Figure S1. Comparison of CMIP5 simulations of global land surface temperature (°C)to observations from the HadCRUT5 data set. Fig. S1 shows the CMIP5-based difference that is estimated by the simulated historical temperature minus the observed temperature for the period of 1986 – 2005.

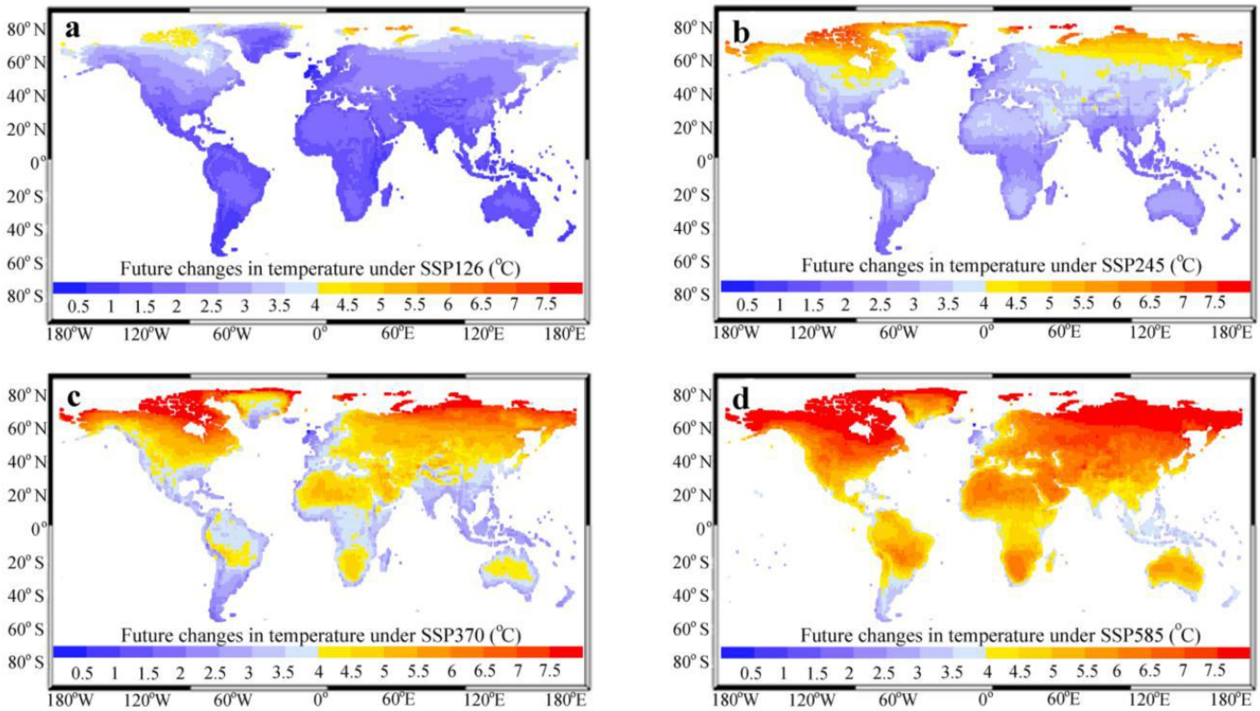

Figure S2. Changes in future land surface temperature based on CMIP6 models. Panels (**a**), (**b**), (**c**) and (**d**) show the CMIP6 multi-model median change in 20-year return values of global annual average land surface temperature as simulated by CMIP6 models in 2081 – 2100 relative to 1986 – 2005 for the emission scenarios of SSP126, SSP245, SSP370 and SSP585, respectively.

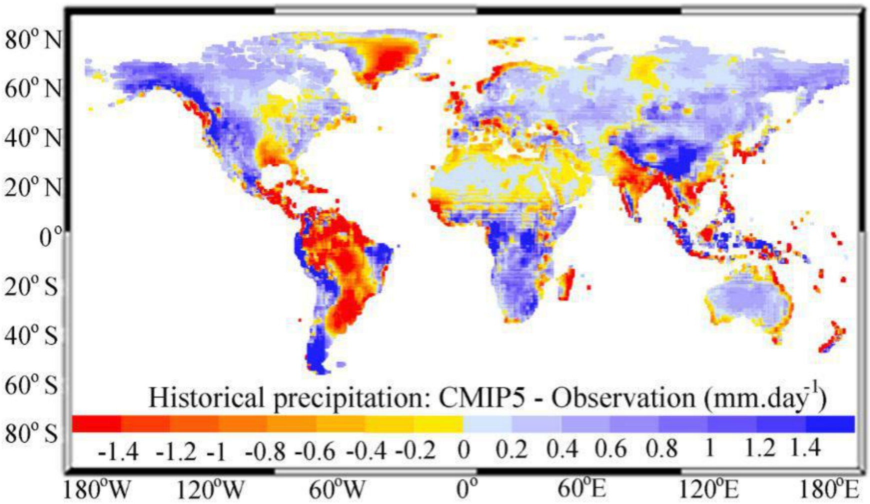

Figure S3. Compariosn of CMIP5 simulations global precipitation (mm day^{-1}) with to observations from the HadCRUT5 data set. Fig. S2 shows the CMIP5-based difference that is estimated by the simulated historical precipitation minus the observed precipitation for the period of 1986 – 2005.

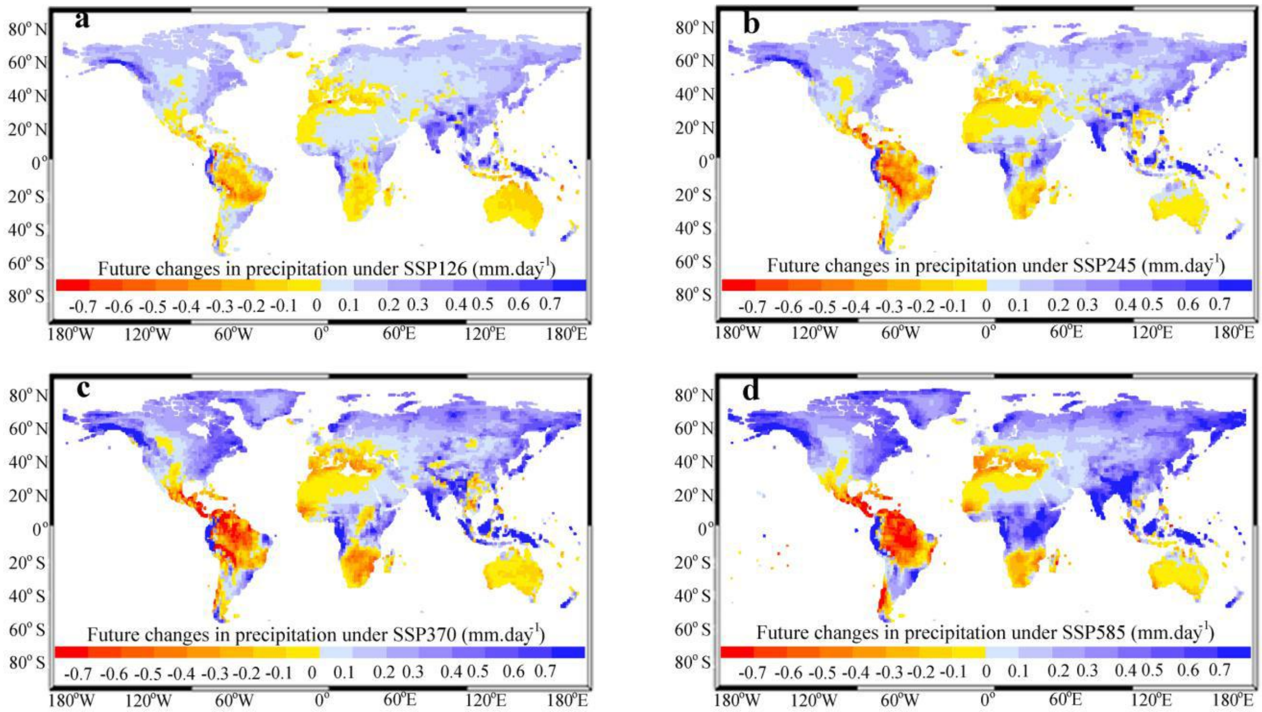

Figure S4. Changes in future precipitation based on CMIP6 models. (**a**), (**b**), (**c**) and (**d**) are the CMIP6 multi-model median change in 20-year return values of global annual average land surface precipitation as simulated by CMIP6 models in 2081 – 2100 relative to 1986 – 2005 for the emission scenarios of SSP126, SSP245, SSP370 and SSP585, respectively.

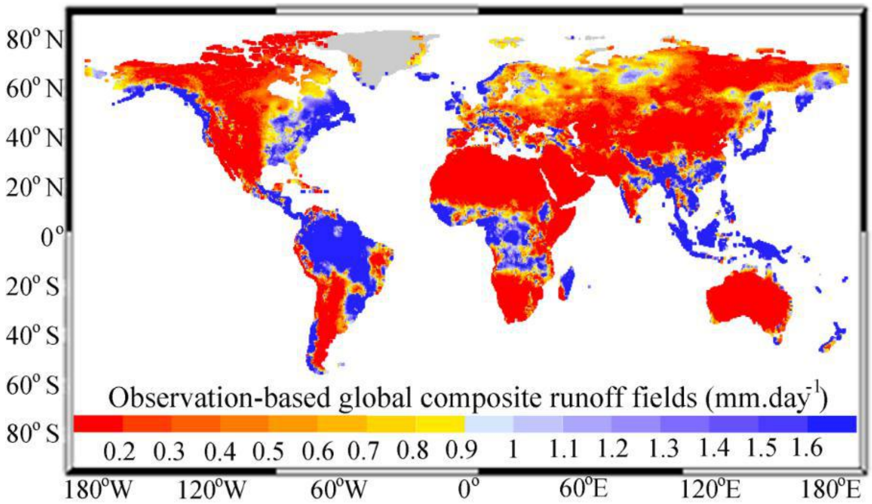

Figure S5. Observation-based Global Composite Runoff Fields from the Global Runoff Data Centre.

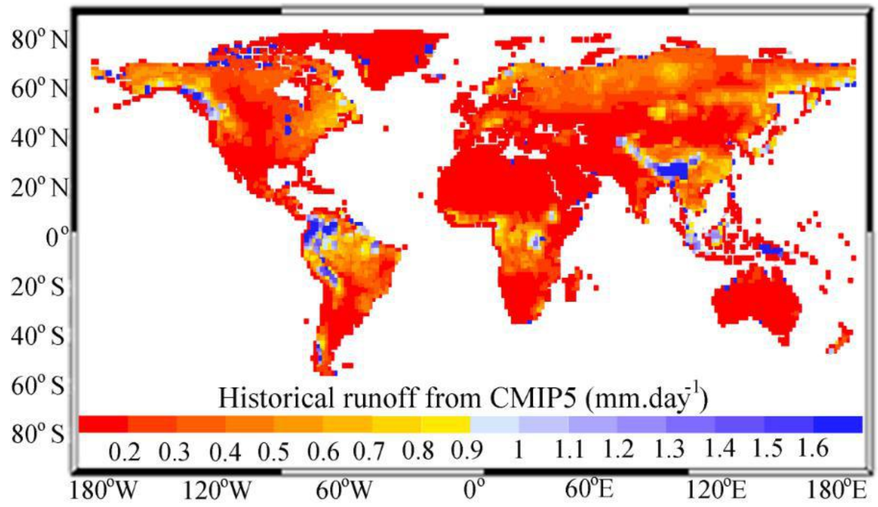

Figure S6. CMIP5-based distribution of the global land surface mean runoff over the period of 1986 – 2005.

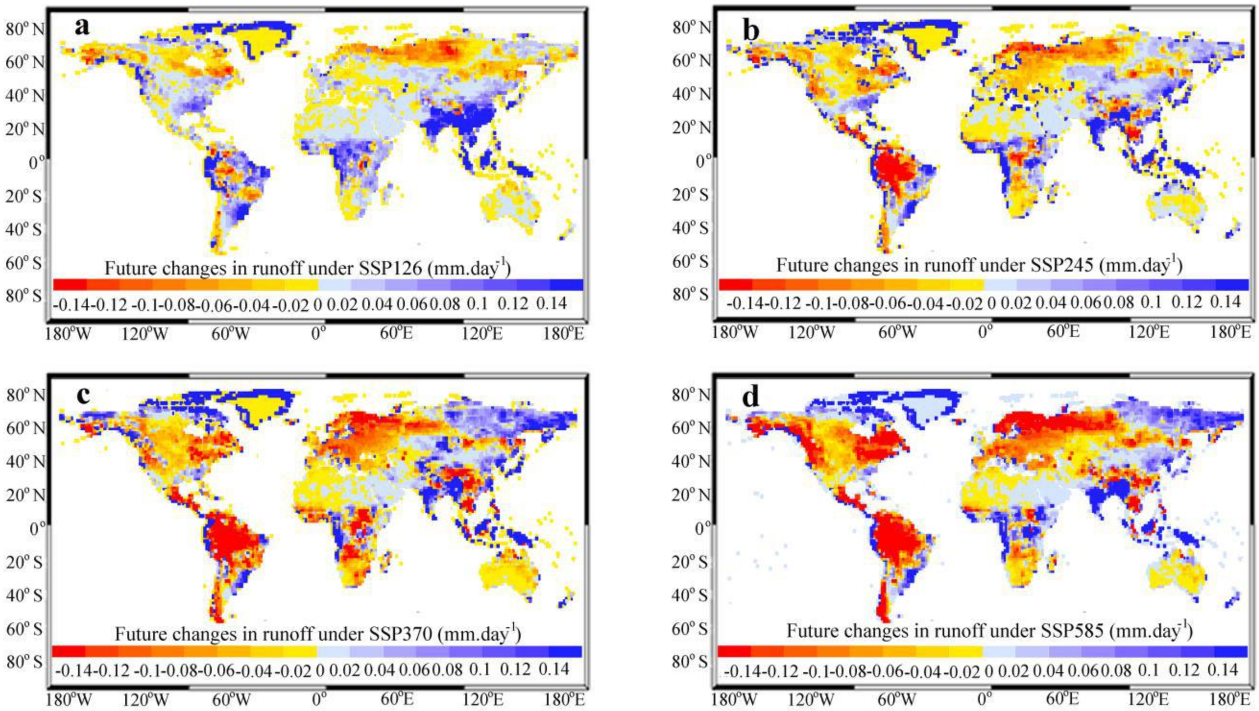

Figure S7. Changes in future land surface runoff based on CMIP6 models. Panels (**a**), (**b**), (**c**) and (**d**) are the CMIP6 multi-model median change in 20-year return values of global annual average land surface runoff as simulated by CMIP6 models in 2081 – 2100 relative to 1986 – 2005 for the emission scenarios of SSP126, SSP245, SSP370 and SSP585, respectively.

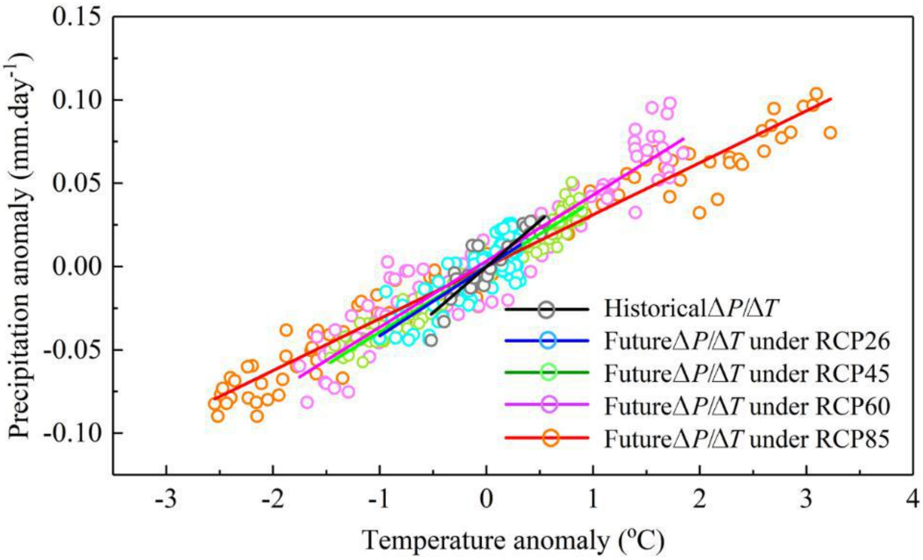

Figure S8. Estimated global $\Delta P/\Delta T$ (mm day^{-1} °C^{-1}) based on CMIP5 model simulations. Fig. S8 shows the linear regression relations between annual average daily precipitation and annual average land surface temperature based on CMIP5 outputs for the historical period of 1979 – 2014 (P=0.0550T, r=0.90, *p value*<0.001), and for the future period of 2015 – 2100 under RCP26 (P=0.0414T, r=0.81, *p value*<0.001), RCP45 (P=0.0392T, r=0.97, *p value*<0.001), RCP60 (P=0.0397T, r=0.95, *p value*<0.001) and RCP85 (P=0.0312T, r=0.98, *p value*<0.001).

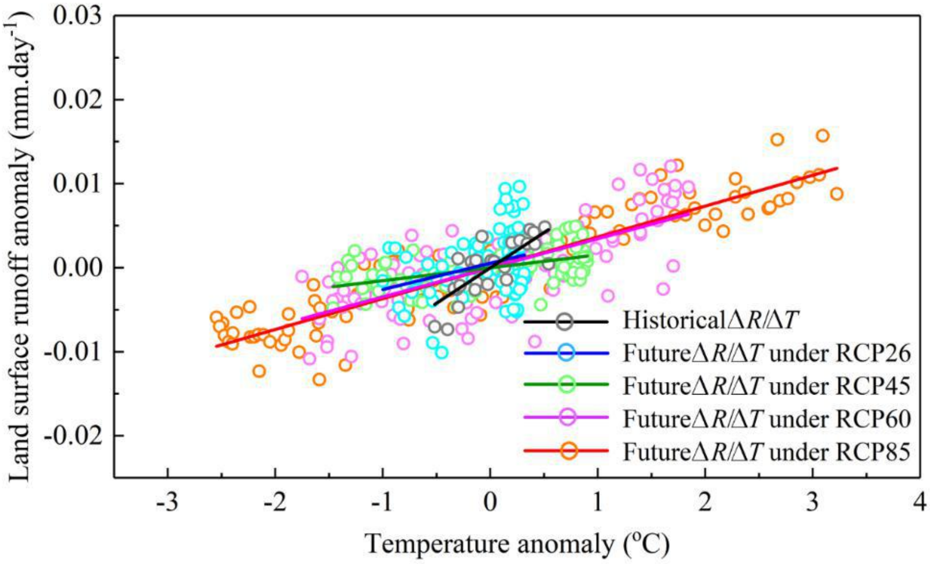

Figure S9. Simulated global $\Delta R/\Delta T$ (mm day^{-1} °C^{-1}) based on CMIP5 models. Fig. S9 shows the linear regression relations between runoff and temperature based on CMIP5 outputs for the historical period of 1979 – 2014 (R=0.0084T, r=0.77, *p value*<0.001), and for the future period of 2015 – 2100 under RCP26 (R=0.0031T, r=0.29, *p value*<0.005), RCP45 (R=0.0015T, r=0.51, *p value*<0.001), RCP60 (R=0.0035T, r=0.70, *p value*<0.001) and RCP85 (R=0.0037T, r=0.92, *p value*<0.001).

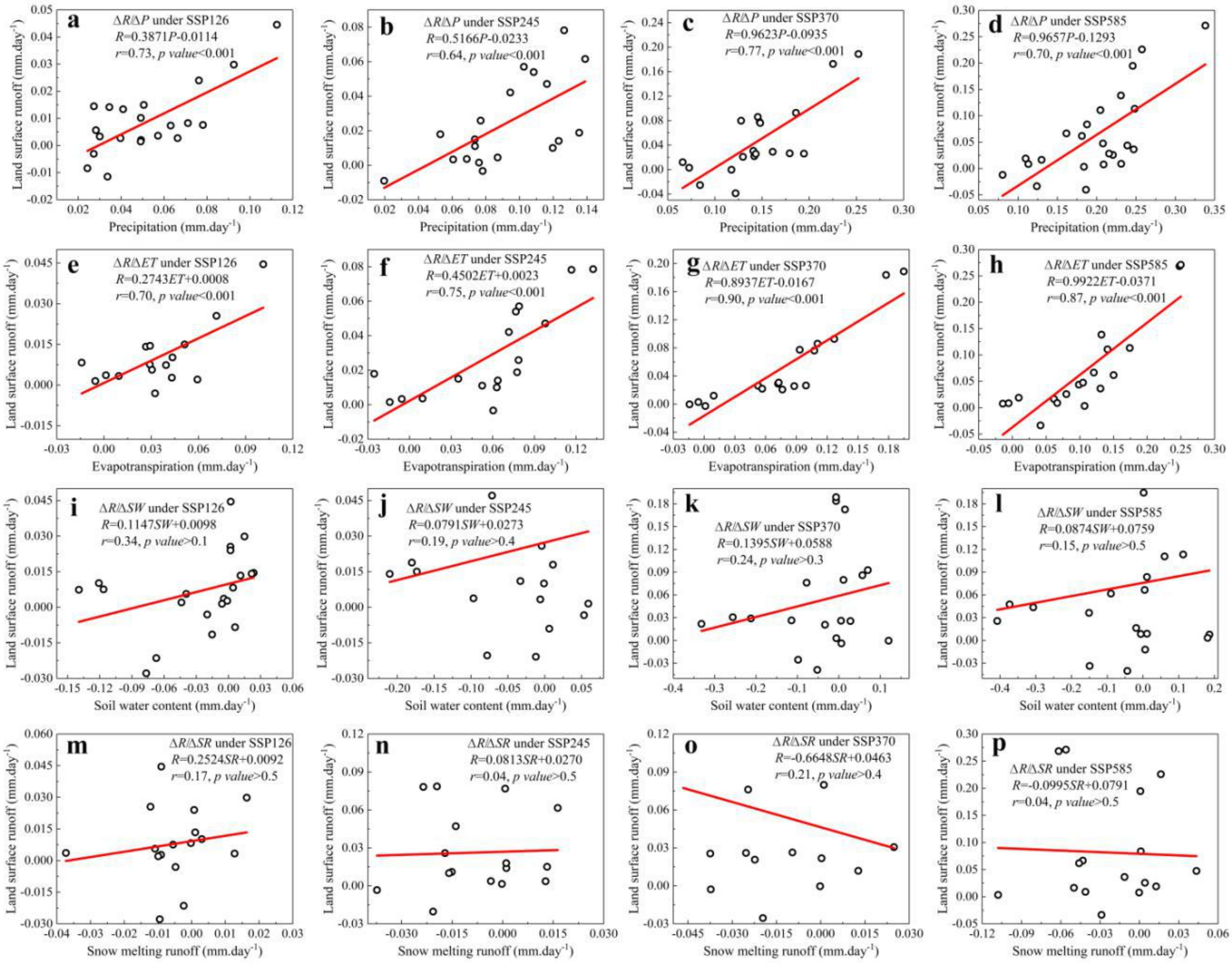

Figure S10. Linear regression relations between the future land surface runoff changes (mm day^{-1}) and the future main climatic factors changes (mm day^{-1}) from 2015–2014 to 2091–2100 based on CMIP6 projections. Panels (**a**), (**b**), (**c**) and (**d**) show the relations between the future land surface runoff changes (Δ*R*) and the future precipitation changes (Δ*P*) under SSP126, SSP245, SSP370 and SSP585, respectively. Similarly panels (**e**), (**f**), (**g**) and (**h**) show the relations between the future land surface runoff changes (Δ*R*) and the future evapotranspiration changes (Δ*ET*). (**i**), (**j**), (**k**) and (**l**) are the relations between the future land surface runoff changes (Δ*R*) and the future soil water content changes (Δ*SW*). Panels (**m**), (**n**), (**o**) and (**p**) show the relations between the future land surface runoff changes (Δ*R*) and the future snow runoff melting runoff changes (Δ*SR*).

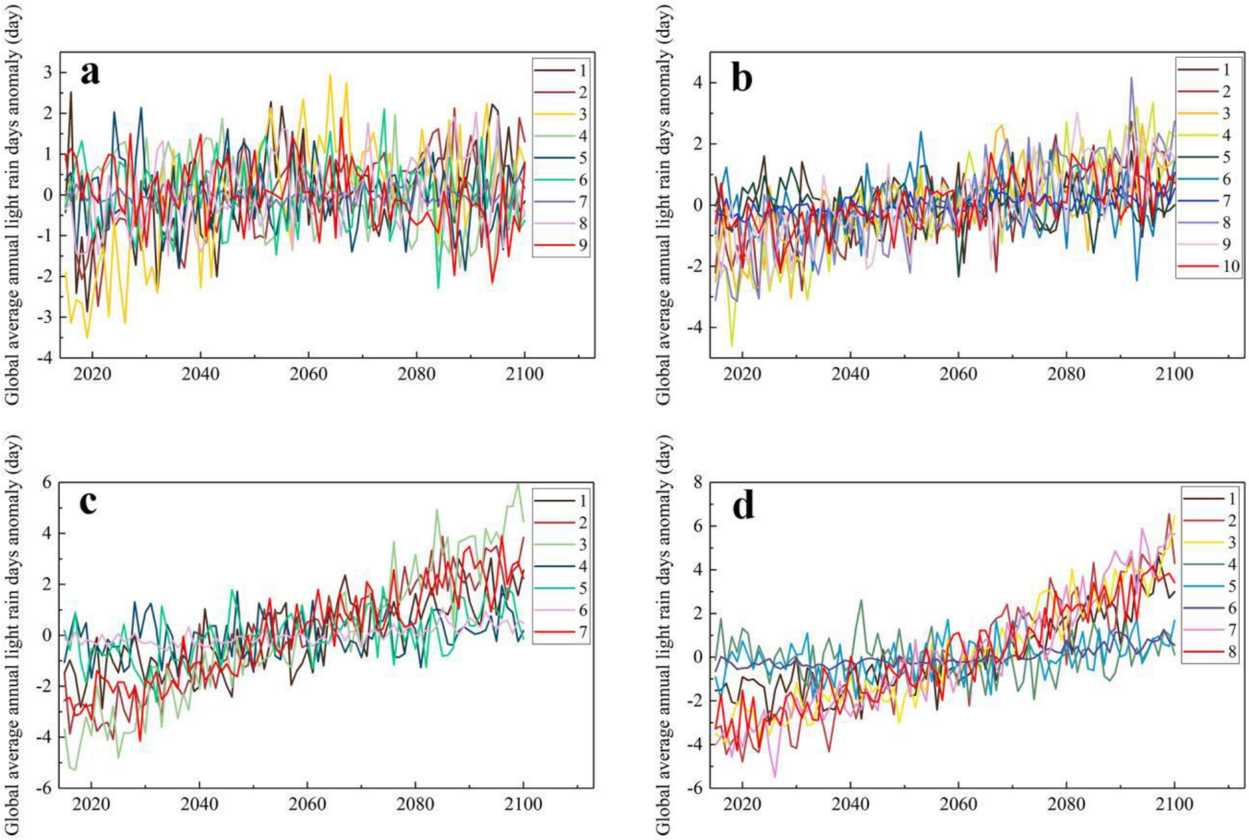

Figure S11. Future changes in global average annual light rain days during 2015-2100 based on the outputs from the 12 CMIP6 models. (a), (b), (c) and (d) are the trends for the emission scenarios under SSP126, SSP245, SSP370 and SSP585, respectively. Each number represents a CMIP6 model (See full name in Table S6)

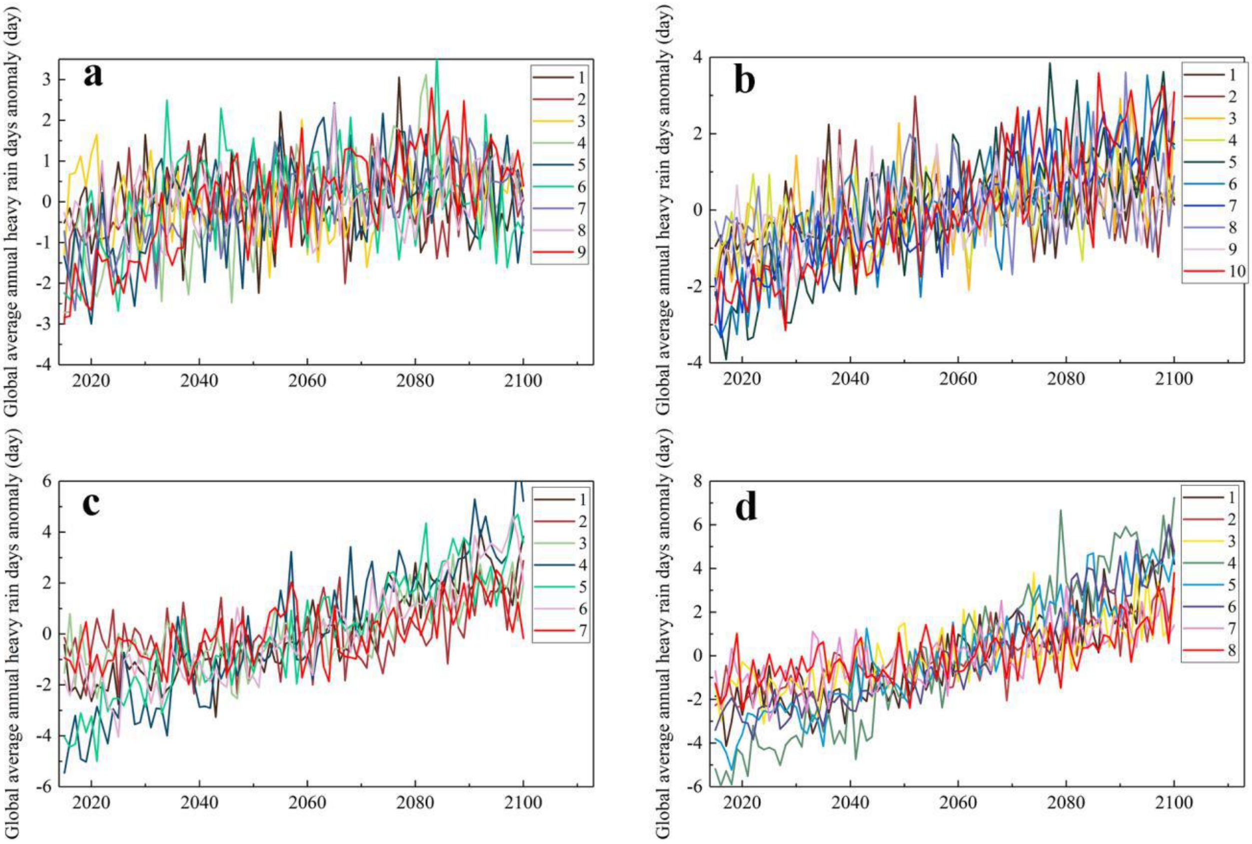

Figure S12. Future changes in global average annual heavy rainfall days during 2015-2100 based on the outputs from the 12 CMIP6 models. Panels (a), (b), (c) and (d) show the trends for the emission scenarios under SSP126, SSP245, SSP370 and SSP585, respectively. Each number represents a CMIP6 model (See full name in Table S6)

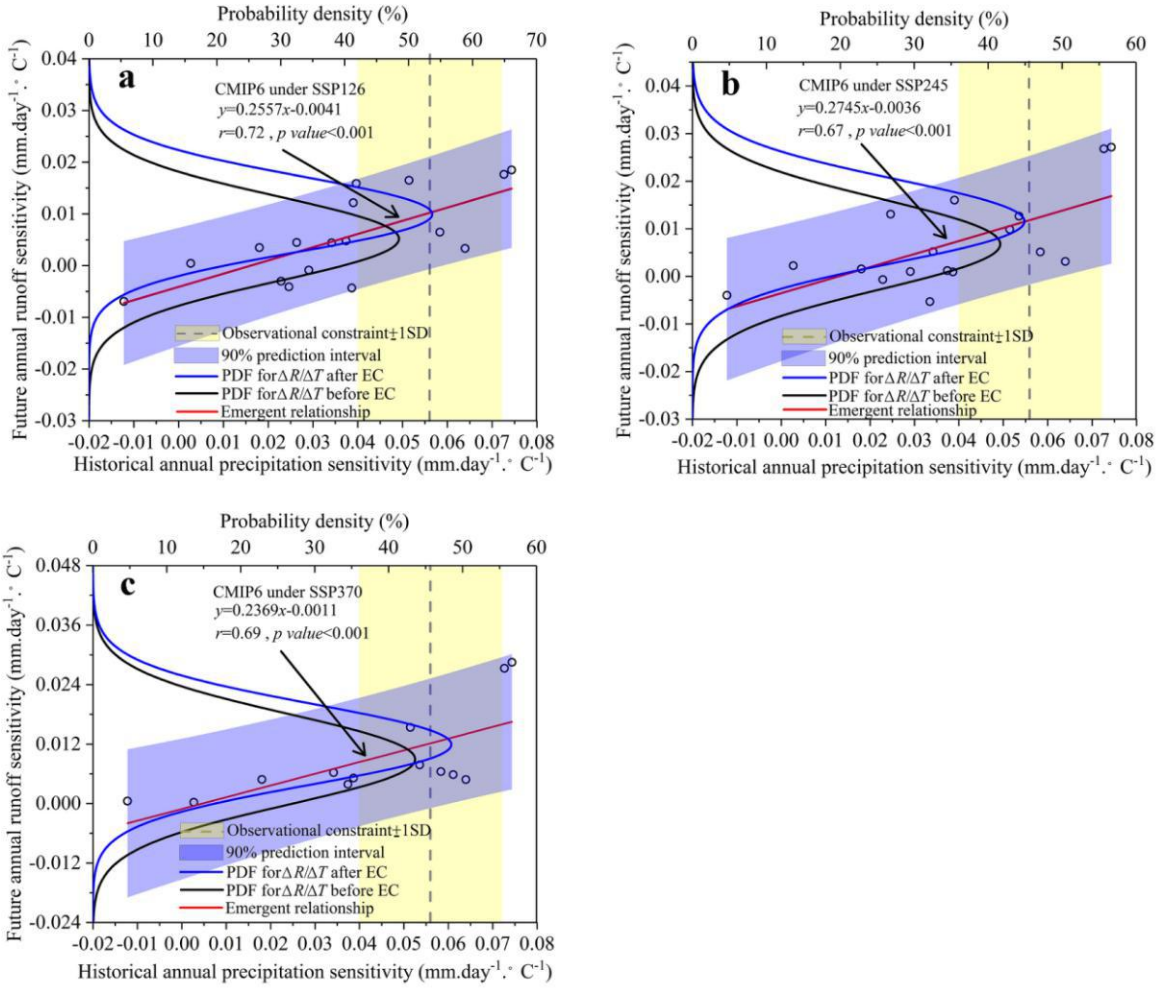

Figure. S13 Emergent constraint on the future sensitivity of global land surface runoff to temperature based on CMIP6 projections. (a), (b) and (c) are the emergent constraint for the outputs from CMIP6 models under SSP126, SSP245 and SSP370 respectively. Note: red line is the linear regression relationship between "the sensitivity of the future global annual land surface runoff to temperature during 2015-2100 (see left y-axis)" and "the sensitivity of the historical global annual precipitation to temperature during 1979-2014 (see bottom x-axis)"; yellow shading is the observational precipitation sensitivity from the HadCRUT5 (observed value ± 1 standard error, 0.056 ± 0.016 mm.day^{-1}.°C^{-1}). The blue shading is the 90% prediction error of the linear fitting; black line and blue line are the probability density functions (PDFs, see top x-axis and left y-axis) for the future global annual runoff sensitivities before and after emergent constraint, by assuming all models are following by Gaussian distribution (*See method for PDF calculation*);

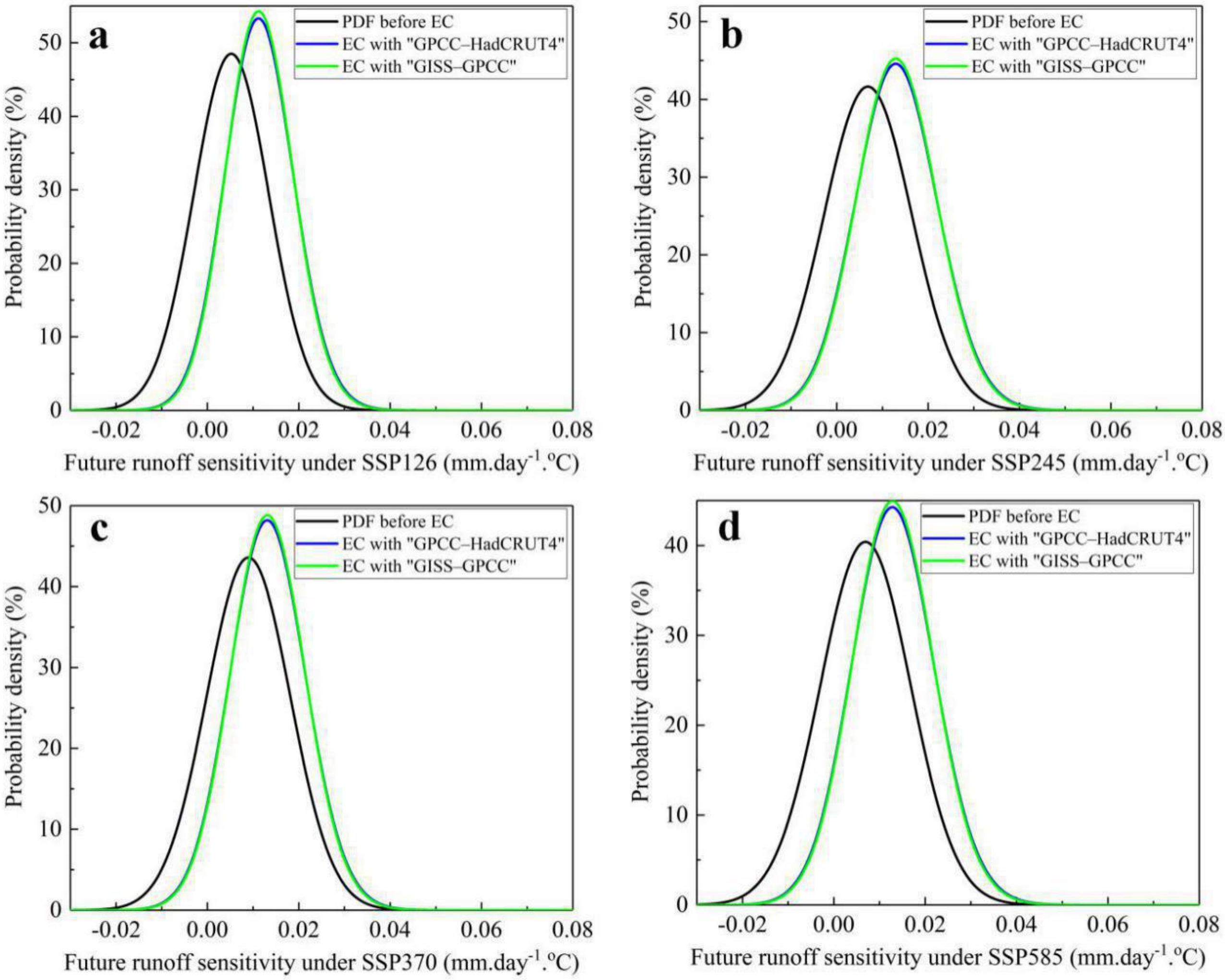

Figure. S14 Emergent constraint (EC) on the future annual runoff sensitivity from CMIP6 projections based on the datasets of "GPCC–HadCRUT5" and "GISS–GPCC". These PDFs are respectively deduced from **a,** the SSP126 scenario, **b,** the SSP245 scenario, **c,** the SSP370 scenario, and **d,** the SSP585 scenario.

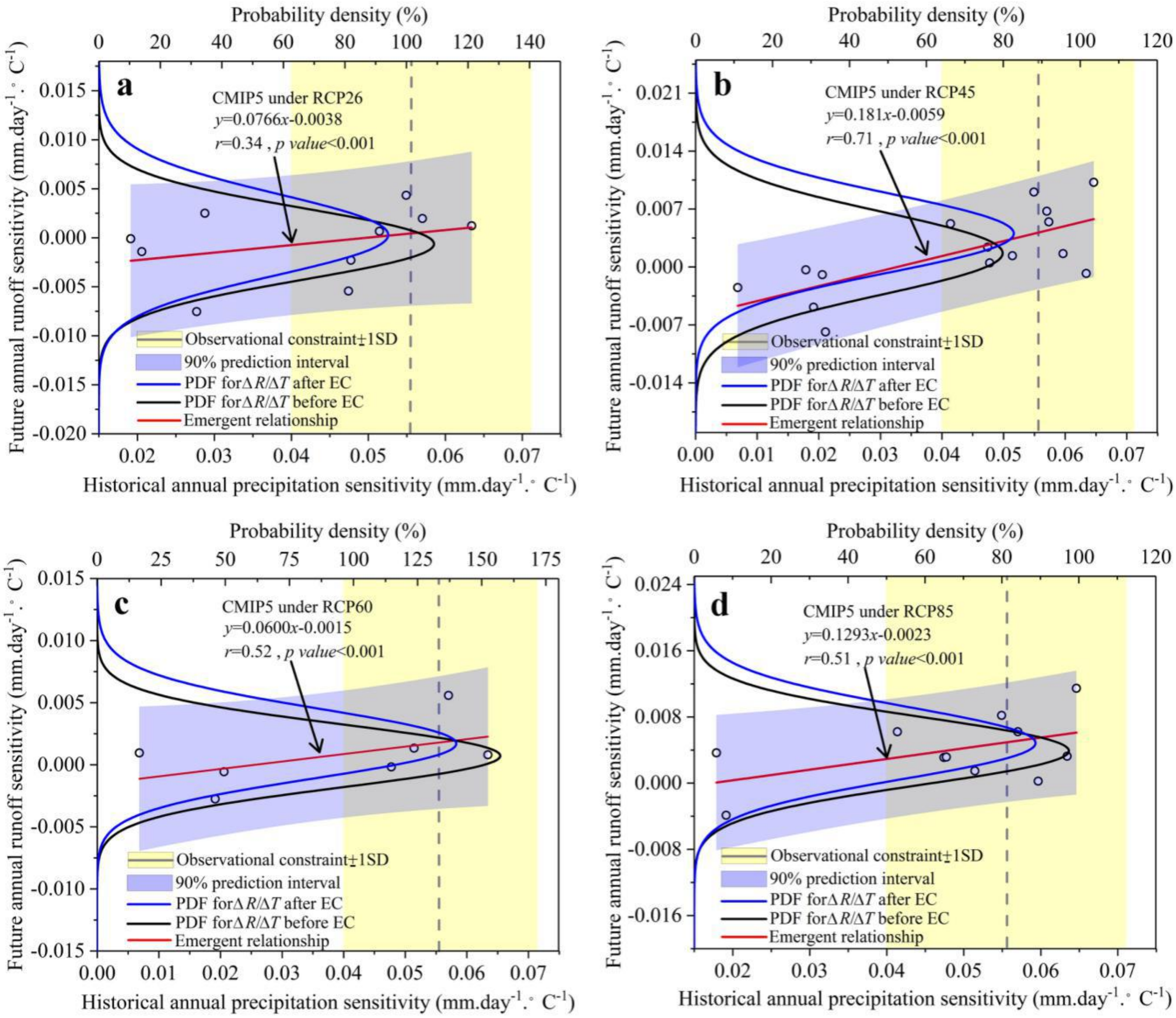

Figure. S15 Emergent constraint on the future sensitivity of global land surface runoff to temperature based on CMIP5 projections. (**a**), (**b**), (**c**) and (**d**) are the emergent constraint for the outputs from CMIP5 models under RCP26, RCP45, RCP60 and RCP85 respectively. Note: red line is the linear regression relationship between "the sensitivity of the future global annual land surface runoff to temperature during 2006-2100 (see left y-axis)" and "the sensitivity of the historical global annual precipitation to temperature during 1979-2005 (see bottom x-axis)"; yellow shading is the observational precipitation sensitivity from the HadCRUT5 (observed value ± 1 standard error). The blue shading is the 90% prediction error of the linear fitting; black line and blue line are the probability density functions (PDFs, see top x-axis and left y-axis) for the future global annual runoff sensitivities before and after emergent constraint, by assuming all models are following by Gaussian distribution;

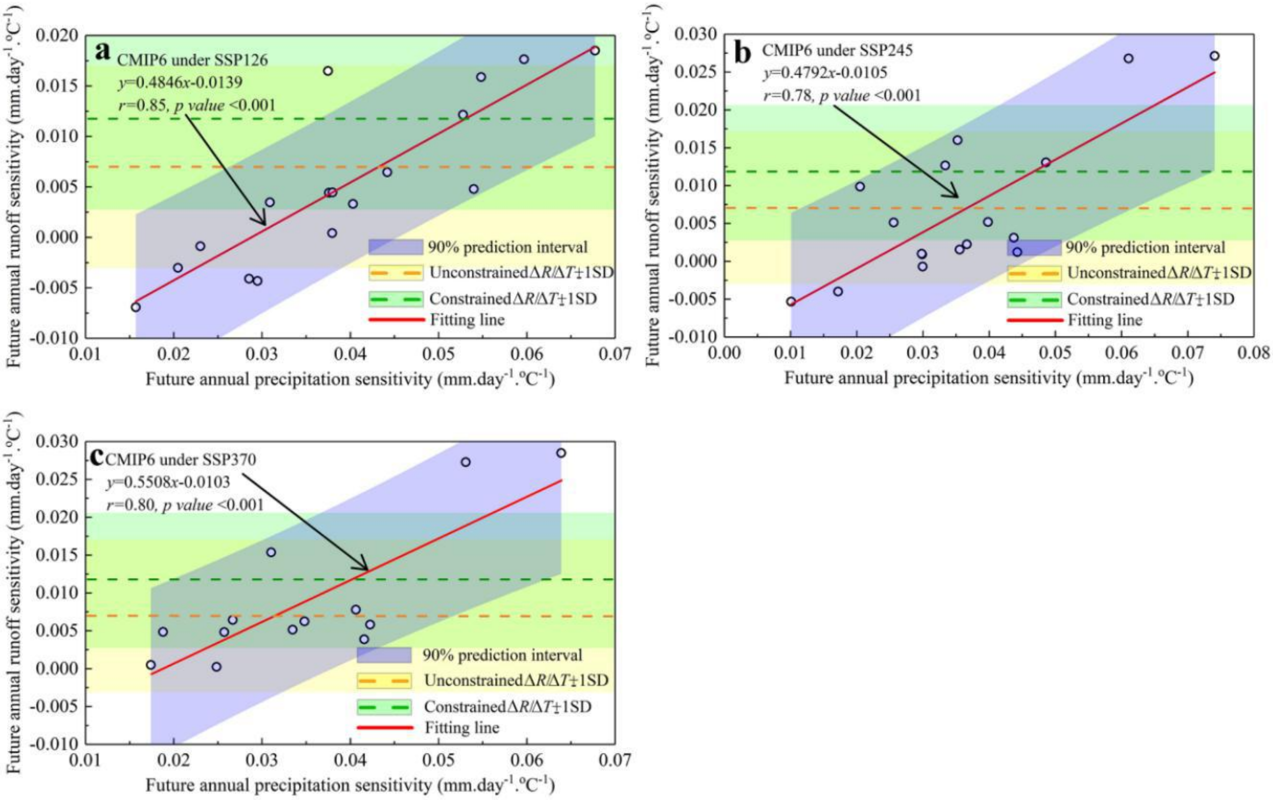

Figure S16. Linear relationships between future annual $\Delta P/\Delta T$ and $\Delta R/\Delta T$ for the CMIP6 models under the emission scenarios of SSP126, SSP245 and SSP370.

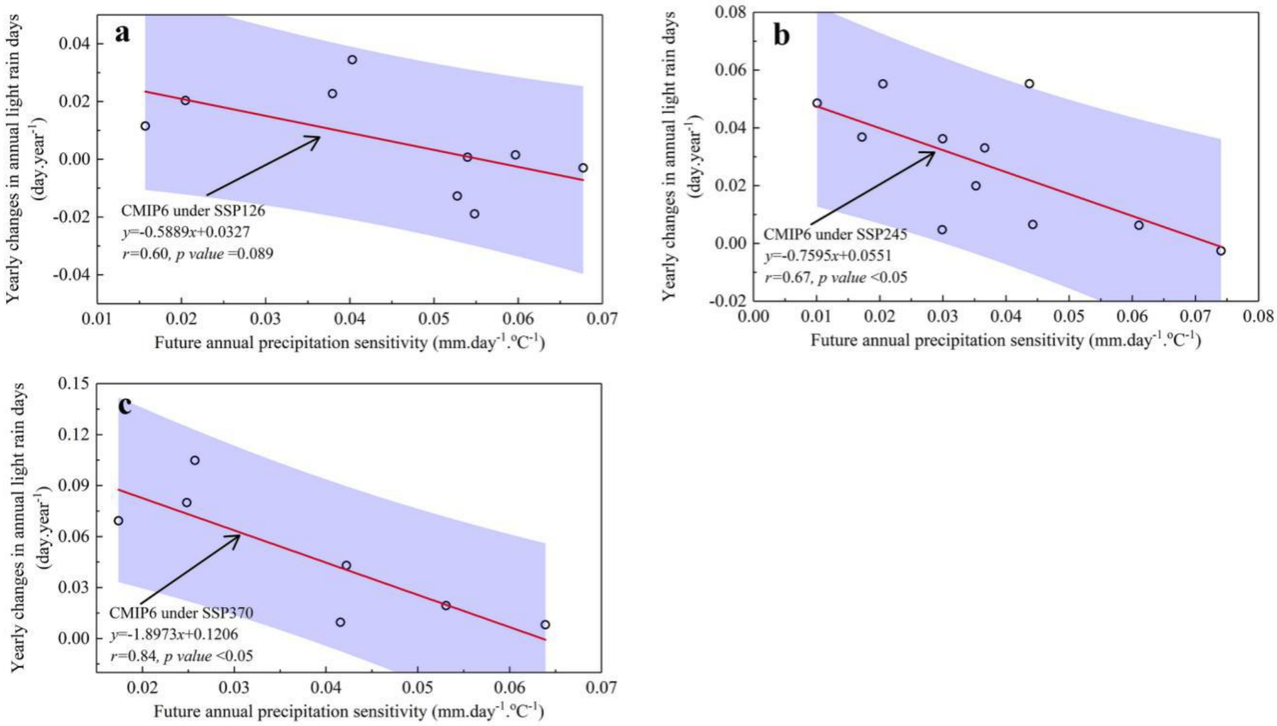

Figure. S17 Constraint on the future yearly changes in global average annual drought days using the constrained future annual runoff sensitivity. Panels (a), (b) and (c) are the constraint for the emission scenarios under SSP126, SSP245 and SSP370, respectively. Note: red line is the linear regression relationship between "future yearly changes in global average annual drought days during 2015-2100 (see left y-axis)" and "the sensitivity of the future global annual runoff to temperature during 2015-2100 (see bottom x-axis)"; yellow shading is the constrained future global annual runoff using the HadCRUT5 (observed value ± 1 standard error, 0.0117 ± 0.009 mm day^{-1} $°C^{-1}$). The blue shading is the 90% prediction error of the linear fitting; black line and blue line are the probability density functions (PDFs, see top x-axis and left y-axis) for the future yearly changes in global average annual drought days before and after constraint, by assuming all models are following by Gaussian distribution;

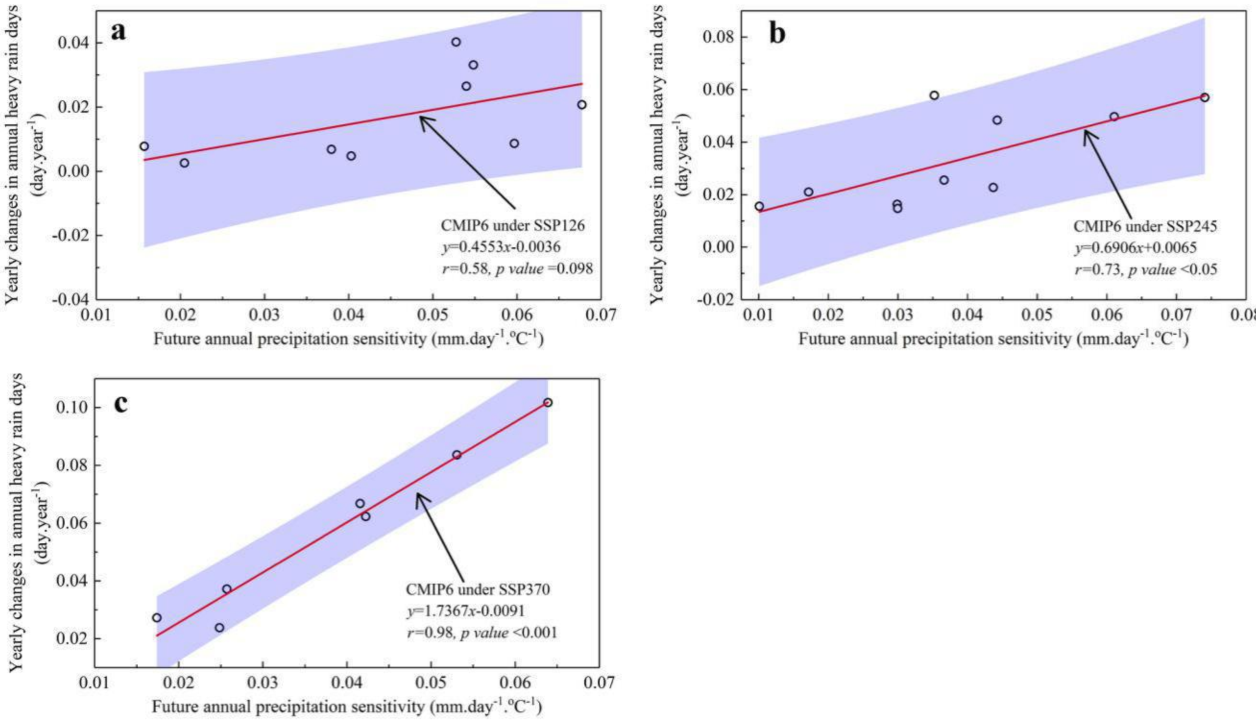

Figure. S18 Constraint on the future yearly changes in global average annual heavy rainfall days using the constrained future annual runoff sensitivity. Panels (a), (b) and (c) are the constraint for the emission scenarios under SSP126, SSP245 and SSP370, respectively. Note: red line is the linear regression relationship between "future yearly changes in global average annual heavy rainfall days during 2015-2100 (see left y-axis)" and "the sensitivity of the future global annual runoff to temperature during 2015-2100 (see bottom x-axis)"; yellow shading is the constrained future global annual runoff using the HadCRUT5 (observed value ± 1 standard error, 0.0117 ± 0.009 mm day^{-1} °C^{-1}). The blue shading is the 90% prediction error of the linear fitting; black line and blue line are the probability density functions (PDFs, see top x-axis and left y-axis) for the future yearly changes in global average annual heavy rainfall days before and after constraint, by assuming all models are following by Gaussian distribution;

Table S1. Full name of the 21 CMIP6 models used for the data of monthly precipitation, runoff and temperature during the historical period (1979–2014) and the future period (2015–2100).

	Precipitation / Runoff / Temperature				
Number	Historical period	Future period under SSP126	Future period under SSP245	Future period under SSP370	Future period under SSP585
1	ACCESS-CM2	BCC-CSM2-MR	BCC-CSM2-MR	ACCESS-CM2	ACCESS-CM2
2	ACCESS-ESM1-5	CESM2	CESM2	BCC-CSM2-MR	ACCESS-ESM1-5
3	BCC-CSM2-MR	CESM2-WACCM	CESM2-WACCM	CESM2	BCC-CSM2-MR
4	CESM2	CNRM-CM6-1	CNRM-CM6-1	CNRM-CM6-1	CESM2
5	CESM2-WACCM	CNRM-CM6-1-HR	CNRM-CM6-1-HR	CNRM-CM6-1-HR	CESM2-WACCM
6	CNRM-CM6-1	CNRM-ESM2-1	CNRM-ESM2-1	CNRM-ESM2-1	CNRM-CM6-1
7	CNRM-CM6-1-HR	FIO-ESM-2-0	FIO-ESM-2-0	GISS-E2-1-G	CNRM-CM6-1-HR
8	CNRM-ESM2-1	GISS-E2-1-G	GISS-E2-1-G	INM-CM4-8	CNRM-ESM2-1
9	FIO-ESM-2-0	HadGEM3-GC31-LL	INM-CM4-8	INM-CM5-0	FIO-ESM-2-0
10	GISS-E2-1-G	INM-CM4-8	INM-CM5-0	IPSL-CM6A-LR	GISS-E2-1-G
11	HadGEM3-GC31-LL	INM-CM5-0	IPSL-CM6A-LR	MIROC6	INM-CM4-8
12	INM-CM4-8	IPSL-CM6A-LR	MIROC6	MPI-ESM1-2-LR	INM-CM5-0
13	INM-CM5-0	MCM-UA-1-0	MIROC-ES2L	NorESM2-MM	IPSL-CM6A-LR
14	IPSL-CM6A-LR	MIROC-ES2L	MPI-ESM1-2-LR		MIROC6
15	MCM-UA-1-0	MPI-ESM1-2-LR	NorESM2-LM		MIROC-ES2L
16	MIROC6	NorESM2-MM	NorESM2-MM		NorESM2-LM
17	MIROC-ES2L	UKESM1-0-LL	UKESM1-0-LL		NorESM2-MM
18	MPI-ESM1-2-LR				
19	NorESM2-LM				
20	NorESM2-MM				
21	UKESM1-0-LL				

Table S2. Full name of the 17 CMIP5 models used for the data of monthly precipitation, runoff and temperature

	Precipitation / Runoff / Temperature				
Number	Historical period	Future period under RCP26	Future period under RCP45	Future period under RCP60	Future period under RCP85
1	ACCESS1-0	CNRM-CM5	ACCESS1-0	CSIRO-Mk3-6-0	ACCESS1-0
2	CNRM-CM5	CSIRO-Mk3-6-0	CNRM-CM5	GISS-E2-R	CNRM-CM5
3	CSIRO-Mk3-6-0	GISS-E2-R	CSIRO-Mk3-6-0	IPSL-CM5A-MR	CSIRO-Mk3-6-0
4	CSIRO-Mk3L-1-2	IPSL-CM5A-MR	CSIRO-Mk3L-1-2	MIROC-ESM	GISS-E2-H-CC
5	GISS-E2-H-CC	MIROC5	GISS-E2-H-CC	MIROC-ESM-CHEM	GISS-E2-R
6	GISS-E2-R	MIROC-ESM	GISS-E2-R	NorESM1-M	inmcm4
7	GISS-E2-R-CC	MIROC-ESM-CHEM	GISS-E2-R-CC	NorESM1-ME	IPSL-CM5A-MR
8	inmcm4	MPI-ESM-LR	inmcm4		IPSL-CM5B-LR
9	IPSL-CM5A-MR	MPI-ESM-MR	IPSL-CM5A-MR		MIROC-ESM
10	IPSL-CM5B-LR	NorESM1-M	IPSL-CM5B-LR		MIROC-ESM-CHEM
11	MIROC5		MIROC-ESM		MPI-ESM-MR
12	MIROC-ESM		MIROC-ESM-CHEM		
13	MIROC-ESM-CHEM		MPI-ESM-MR		
14	MPI-ESM-LR		NorESM1-M		
15	MPI-ESM-MR		NorESM1-ME		
16	NorESM1-M				
17	NorESM1-ME				

Table S3. Full name of the 16 CMIP6 models used for the data of monthly snow melt

	Snow melting runoff				
Number	Historical period	Future period under SSP126	Future period under SSP245	Future period under SSP370	Future period under SSP585
1	ACCESS-CM2	ACCESS-CM2	ACCESS-CM2	ACCESS-CM2	ACCESS-CM2
2	ACCESS-ESM1-5	ACCESS-ESM1-5	ACCESS-ESM1-5	ACCESS-ESM1-5	ACCESS-ESM1-5
3	BCC-CSM2-MR	BCC-CSM2-MR	BCC-CSM2-MR	BCC-CSM2-MR	BCC-CSM2-MR
4	CanESM5	CanESM5	CanESM5	CanESM5	CanESM5
5	CanESM5-CanOE	CanESM5-CanOE	CanESM5-CanOE	CanESM5-CanOE	CanESM5-CanOE
6	CESM2	CESM2	CESM2	CESM2	CESM2
7	CESM2-WACCM	CESM2-WACCM	CESM2-WACCM	CESM2-WACCM	CESM2-WACCM
8	CNRM-CM6-1	CNRM-CM6-1	CNRM-CM6-1	CNRM-CM6-1	CNRM-CM6-1
9	CNRM-ESM2-1	CNRM-ESM2-1	CNRM-ESM2-1	CNRM-ESM2-1	CNRM-ESM2-1
10	GISS-E2-1-G	GISS-E2-1-G	GISS-E2-1-G	GISS-E2-1-G	GISS-E2-1-G
11	HadGEM3-GC31-LL	HadGEM3-GC31-LL	HadGEM3-GC31-LL	IPSL-CM6A-LR	HadGEM3-GC31-LL
12	IPSL-CM6A-LR	IPSL-CM6A-LR	IPSL-CM6A-LR	MIROC6	IPSL-CM6A-LR
13	MIROC6	MIROC6	MIROC6	MIROC-ES2L	MIROC6
14	MIROC-ES2L	MIROC-ES2L	MIROC-ES2L	MPI-ESM1-2-LR	MIROC-ES2L
15	MPI-ESM1-2-LR	MPI-ESM1-2-LR	MPI-ESM1-2-LR	UKESM1-0-LL	MPI-ESM1-2-LR
16	UKESM1-0-LL	UKESM1-0-LL	UKESM1-0-LL		UKESM1-0-LL

Table S4. Full name of the 21 CMIP6 models used for the data of monthly soil water content

	Soil water content				
Number	Historical period	Future period under SSP126	Future period under SSP245	Future period under SSP370	Future period under SSP585
1	ACCESS-CM2	ACCESS-CM2	ACCESS-CM2	ACCESS-CM2	ACCESS-CM2
2	ACCESS-ESM1-5	ACCESS-ESM1-5	ACCESS-ESM1-5	ACCESS-ESM1-5	ACCESS-ESM1-5
3	BCC-CSM2-MR	BCC-CSM2-MR	BCC-CSM2-MR	BCC-CSM2-MR	BCC-CSM2-MR
4	CanESM5	CanESM5	CanESM5	CanESM5	CanESM5
5	CanESM5-CanOE	CanESM5-CanOE	CanESM5-CanOE	CanESM5-CanOE	CanESM5-CanOE
6	CESM2	CESM2	CESM2	CESM2	CESM2
7	CESM2-WACCM	CESM2-WACCM	CESM2-WACCM	CNRM-CM6-1	CESM2-WACCM
8	CNRM-CM6-1	CNRM-CM6-1	CNRM-CM6-1	CNRM-CM6-1-HR	CNRM-CM6-1
9	CNRM-CM6-1-HR	CNRM-CM6-1-HR	CNRM-CM6-1-HR	CNRM-ESM2-1	CNRM-CM6-1-HR
10	CNRM-ESM2-1	CNRM-ESM2-1	CNRM-ESM2-1	INM-CM4-8	CNRM-ESM2-1
11	HadGEM3-GC31-LL	HadGEM3-GC31-LL	HadGEM3-GC31-LL	INM-CM5-0	HadGEM3-GC31-LL
12	INM-CM4-8	INM-CM4-8	INM-CM4-8	IPSL-CM6A-LR	INM-CM4-8
13	INM-CM5-0	INM-CM5-0	INM-CM5-0	MIROC6	INM-CM5-0
14	IPSL-CM6A-LR	IPSL-CM6A-LR	IPSL-CM6A-LR	MIROC-ES2L	IPSL-CM6A-LR
15	MIROC6	MIROC6	MIROC6	MPI-ESM1-2-LR	MIROC6
16	MIROC-ES2L	MIROC-ES2L	MIROC-ES2L	MRI-ESM2-0	MIROC-ES2L
17	MPI-ESM1-2-LR	MPI-ESM1-2-LR	MPI-ESM1-2-LR	NorESM2-LM	MPI-ESM1-2-LR
18	MRI-ESM2-0	MRI-ESM2-0	MRI-ESM2-0	NorESM2-MM	MRI-ESM2-0
19	NorESM2-LM	NorESM2-LM	NorESM2-LM	UKESM1-0-LL	NorESM2-LM
20	NorESM2-MM	NorESM2-MM	NorESM2-MM		NorESM2-MM
21	UKESM1-0-LL	UKESM1-0-LL	UKESM1-0-LL		UKESM1-0-LL

Table S5. Full name of the 19 CMIP6 models used for the data of monthly total evaporation

Number	Total evaporation				
	Historical period	Future period under SSP126	Future period under SSP245	Future period under SSP370	Future period under SSP585
1	ACCESS-CM2	BCC-CSM2-MR	BCC-CSM2-MR	ACCESS-CM2	ACCESS-CM2
2	ACCESS-ESM1-5	CanESM5	CanESM5-CanOE	BCC-CSM2-MR	ACCESS-ESM1-5
3	BCC-CSM2-MR	CanESM5-CanOE	CESM2	CanESM5-CanOE	BCC-CSM2-MR
4	CanESM5	CESM2	CESM2-WACCM	CESM2	CanESM5-CanOE
5	CanESM5-CanOE	CESM2-WACCM	CNRM-CM6-1	CESM2-WACCM	CESM2
6	CESM2	CNRM-CM6-1	CNRM-CM6-1-HR	CNRM-CM6-1	CESM2-WACCM
7	CESM2-WACCM	CNRM-CM6-1-HR	CNRM-ESM2-1	CNRM-CM6-1-HR	CNRM-CM6-1
8	CNRM-CM6-1	CNRM-ESM2-1	GISS-E2-1-G	CNRM-ESM2-1	CNRM-CM6-1-HR
9	CNRM-CM6-1-HR	GISS-E2-1-G	INM-CM4-8	GISS-E2-1-G	CNRM-ESM2-1
10	CNRM-ESM2-1	INM-CM4-8	INM-CM5-0	INM-CM4-8	GISS-E2-1-G
11	GISS-E2-1-G	INM-CM5-0	IPSL-CM6A-LR	INM-CM5-0	INM-CM4-8
12	INM-CM4-8	IPSL-CM6A-LR	MCM-UA-1-0	IPSL-CM6A-LR	INM-CM5-0
13	INM-CM5-0	MCM-UA-1-0	MIROC6	MCM-UA-1-0	IPSL-CM6A-LR
14	IPSL-CM6A-LR	MIROC6	MIROC-ES2L	MIROC6	MCM-UA-1-0
15	MCM-UA-1-0	MIROC-ES2L	MPI-ESM1-2-LR	MIROC-ES2L	MIROC6
16	MIROC6	NorESM2-MM	NorESM2-MM	NorESM2-MM	MIROC-ES2L
17	MIROC-ES2L				NorESM2-MM
18	MPI-ESM1-2-LR				
19	NorESM2-MM				

Table S6. Full name of the 10 CMIP6 models used for the data of daily precipitation

	Daily precipitation			
Number	Future period under SSP126	Future period under SSP245	Future period under SSP370	Future period under SSP585
1	CESM2-WACCM	BCC-CSM2-MR	ACCESS-CM2	ACCESS-CM2
2	CESM2	CESM2-WACCM	CESM2	CESM2-WACCM
3	CNRM-ESM2-1	CESM2	CNRM-ESM2-1	CESM2
4	HadGEM3-GC31-LL	CNRM-ESM2-1	INM-CM4-8	INM-CM4-8
5	INM-CM4-8	INM-CM4-8	INM-CM5-0	INM-CM5-0
6	INM-CM5-0	INM-CM5-0	IPSL-CM6A-LR	IPSL-CM6A-LR
7	IPSL-CM6A-LR	IPSL-CM6A-LR	NorESM2-MM	NorESM2-LM
8	NorESM2-MM	NorESM2-LM		NorESM2-MM
9	UKESM1-0-LL	NorESM2-MM		
10		UKESM1-0-LL		

Table S7. Observed annual precipitation sensitivity ($\Delta P/\Delta T$) ± one standard deviation from the four datasets, and predicted annual land surface runoff sensitivity ($\Delta R/\Delta T$) ± one standard deviation based on CMIP6 models before and after emergent constraint.

	Observed precipitation sensitivity ± one standard deviation (mm day^{-1} °C^{-1})	Emission Scenarios	Future runoff sensitivity before emergent constraint (mm day^{-1} °C^{-1})		Future runoff sensitivity after emergent constraint (mm day^{-1} °C^{-1})		Future original runoff changes ± one standard deviation (mm day^{-1})	Future constrained runoff changes ± one standard deviation (mm day^{-1})
			Mean value	one standard deviation	Mean value	one standard deviation		
HadCRUT5	0.056 ± 0.016	SSP126	0.005	0.0082	0.0102	0.0075	0.009±0.009	0.0111±0.0088
		SSP245	0.007	0.0097	0.0119	0.0090	0.019±0.022	0.0300±0.0225
		SSP370	0.009	0.0092	0.0122	0.0081	0.035±0.032	0.0522±0.0342
		SSP585	0.007	0.0100	0.0117	0.0090	0.032±0.039	0.0656±0.0504
HadCRUT5+GPCC	0.061 ± 0.016	SSP126	0.005	0.0082	0.0115	0.0075	0.009±0.009	0.0122±0.0088
		SSP245	0.007	0.0097	0.0132	0.0090	0.019±0.022	0.0325±0.0225
		SSP370	0.009	0.0092	0.0133	0.0081	0.035±0.032	0.0556±0.0342
		SSP585	0.007	0.0100	0.0131	0.0090	0.032±0.039	0.0729±0.0504
GISS+GPCC	0.061 ± 0.015	SSP126	0.005	0.0082	0.0115	0.0075	0.009±0.009	0.0122±0.0077
		SSP245	0.007	0.0097	0.0132	0.0090	0.019±0.022	0.0325±0.0225
		SSP370	0.009	0.0092	0.0133	0.0080	0.035±0.032	0.0556±0.0342
		SSP585	0.007	0.0100	0.0131	0.0090	0.032±0.039	0.0729±0.0560

Table S8. Implications of the unconstrained and the constrained future runoff sensitivities on the future extreme climates

	SSP126 (mm day^{-1} °C^{-1})		SSP245 (mm day^{-1} °C^{-1})		SSP370 (mm day^{-1} °C^{-1})		SSP585 (mm day^{-1} °C^{-1})	
	<-0.0088	>0.0265	<-0.011	>0.0317	<-0.009	>0.0327	<-0.0114	>0.0325
Unconstrained	5%	0%	3%	0%	2%	0%	3%	0%
Constrained	0%	2%	0%	2%	0%	1%	0%	1%